



저작자표시-비영리-변경금지 2.0 대한민국

이용자는 아래의 조건을 따르는 경우에 한하여 자유롭게

- 이 저작물을 복제, 배포, 전송, 전시, 공연 및 방송할 수 있습니다.

다음과 같은 조건을 따라야 합니다:



저작자표시. 귀하는 원저작자를 표시하여야 합니다.



비영리. 귀하는 이 저작물을 영리 목적으로 이용할 수 없습니다.



변경금지. 귀하는 이 저작물을 개작, 변형 또는 가공할 수 없습니다.

- 귀하는, 이 저작물의 재이용이나 배포의 경우, 이 저작물에 적용된 이용허락조건을 명확하게 나타내어야 합니다.
- 저작권자로부터 별도의 허가를 받으면 이러한 조건들은 적용되지 않습니다.

저작권법에 따른 이용자의 권리는 위의 내용에 의하여 영향을 받지 않습니다.

이것은 [이용허락규약\(Legal Code\)](#)을 이해하기 쉽게 요약한 것입니다.

[Disclaimer](#)

공학석사학위논문

건식 스프레이 증착 시스템을 이용한  
유연 열전소자 발전기 상온 제작

Room-temperature fabrication of  
flexible thermoelectric generator  
using dry-spray deposition system

2016년 2월

서울대학교 대학원

기계항공공학부

송 대 섭

## Abstract

# Room-temperature fabrication of flexible thermoelectric generator using dry-spray deposition system

Dae-Seob Song

Department of Mechanical and Aerospace Engineering

The Graduate School

Seoul National University

We present a flexible thermoelectric (TE) generator with titanium dioxide ( $\text{TiO}_2$ ), antimony (Sb), and tellurium (Te) powders fabricated by a nanoparticle deposition system (NPDS). NPDS is a novel low-energy consumption dry-spray method that enables the deposition of inorganic materials on substrates at room temperature and under low vacuum.  $\text{TiO}_2$  nanopowders were dispersed on a TE powder for improved adhesion between TE films and the substrate. Film morphologies were investigated using field-emission scanning electron microscopy, and the phase structure was analyzed by X-ray diffraction. A TE leg, deposited with 3 wt%  $\text{TiO}_2$  content, had the largest Seebeck coefficient of approximately  $160 \mu\text{V/K}$ . The prototype TE generator consisted of 16 TE legs linked by silver interconnects over an area of  $20 \times 60 \text{ mm}^2$ . The prototype produced a voltage of 48.91 mV and a

maximum power output of 0.18  $\mu\text{W}$  from a temperature gradient of 20 K. The values are comparable to that of conventional methods. These results suggest that flexible TE generators can be fabricated by energy efficient methods, although internal and contact resistances must be decreased.

**Keywords:** nano-particle deposition system, flexible thermoelectric generator, dry-spray deposition, room temperature.

**Student Number:** 2014-21841

# Contents

<b>Chapter 1. Introduction.....</b>	<b>1</b>
1.1 Background.....	1
1.2 Fabrication of flexible TE generators .....	2
1.3 Objectives .....	3
<b>Chapter 2. Experimental procedure.....</b>	<b>4</b>
2.1 Nano particle deposition system.....	4
2.2 Materials .....	6
2.3 TE generator fabrication process .....	7
2.4 Characterization.....	8
<b>Chapter 3. Results and Discussion .....</b>	<b>9</b>
3.1 Field-emission scanning electron microscopy.....	9
3.2 X-ray diffraction .....	11
3.3 Seebeck coefficient and internal resistance .....	12
3.4 Prototype flexible TE generator .....	13
3.5 Voltage and power output .....	14
3.6 Comparison with various fabrication methods .....	15

**Chapter 4. Conclusions.....17**

**Reference.....18**

**Abstract (Korean) .....20**

## **List of Tables**

Table 2.1 Nanoparticle deposition system (NPDS) parameters. ....	5
Table 3.1 Comparison of various fabrication processes for flexible TE generators.....	16

## List of Figures

Figure 2.1 Schematic diagram of the nanoparticle deposition system . . . . .	4
Figure 2.2 Schematic diagram of the thermoelectric (TE) generator . . . . .	7
Figure 3.1 Scanning electron microscopy (SEM) images of the surface (top) and cross-section (bottom) of the $\text{TiO}_2/\text{Sb}_2\text{Te}_3$ films. . . . .	10
Figure 3.2 X-ray diffraction (XRD) patterns of the TE powder and the TE films. . . . .	11
Figure 3.3 Seebeck coefficient and internal resistance of one TE leg as a function of the $\text{TiO}_2$ ratio. . . . .	12
Figure 3.4 Image of the flexible TE generator under bending stress . . . . .	13
Figure 3.5 Voltage and power output for the flexible TE power generator as a function of the temperature differential. The inset shows a schematic of the measurement setup. . . . .	14

# **Chapter 1. Introduction**

## **1.1 Background**

Thermoelectric (TE) power generators convert a thermal differential into electrical power and can be used to improve energy consumption efficiency. Moreover, flexible TE power generators can be used in self-powered portable electronic systems, such as wearable electronics, biometric sensors, and autonomous robots [1–4].

## 1.2 Fabrication of flexible TE generator

Recently, various TE materials and manufacturing methods have been developed for the fabrication of flexible TE generators. TE materials based on tellurium (Te) and antimony (Sb) have typically been used for this purpose, due to their high figure of merit values,  $ZT$ , where  $ZT = \alpha^2 \cdot T / \rho \cdot \lambda$ ,  $\lambda$  is the thermal conductivity,  $\rho$  is the electrical resistivity,  $\alpha$  is the Seebeck coefficient, and  $T$  is the temperature; the printing methods utilized (e.g., screen printing [5], inkjet printing [6], metal organic chemical vapor deposition (MOCVD) [7], co-sputtering [8], and flash evaporation [9]) significantly improved the energy conversion efficiency of the TE generators. A glass fabric-based flexible TE generator, which was recently optimized and developed for wearable mobile electronic systems, showed remarkable output power, but also high energy consumption and cost [10]. Pastes which contain TE and binder materials for screen printing and inkjet printing must be annealed. Also, MOCVD consumes a large amount of energy, due to the high growth temperatures required. Co-sputtering and flash evaporation methods require a post-annealing process to improve the TE generator's performance. These high-energy processes negate the benefits of TE generators; thus, more efficient fabrication processes are required for widespread adoption.

### 1.3 Objectives

The nanoparticle deposition system (NPDS), which can deposit metal and ceramic particles using a dry-spray process at room temperature and under low-vacuum conditions, was developed by Ahn et al. in 2006. NPDS is similar to the aerosol deposition method (ADM); however, NPDS is a relatively low-energy consumption process, compared with alternative dry-spray processes [11]. NPDS requires a low-pressure gas carrier and a low vacuum, which reduces energy consumption and the complexity of the facilities needed. NPDS has been used to deposit  $\text{TiO}_2$  and  $\text{WO}_3$  particles on a substrate for energy applications, such as dye-sensitized solar cells (DSSC) and electrochromic displays [12,13], which suggests the use of a NPDS for efficient fabrication of flexible TE generators.

According to a recent study, microparticles with a  $\text{TiO}_2$  nanopowder deposited by NPDS adhered well to the substrate and exhibited a greater film density than other pure microsized particles [14]. In addition,  $\text{TiO}_2$  nanopowders dispersed in TE materials may result in remarkable phonon scattering, reducing thermal conductivity [15].

In the present work, we fabricated 16  $\text{Sb}_2\text{Te}_3$  TE film (p-type) legs, with a  $\text{TiO}_2$  nanopowder, dispersed on a polyvinyl chloride (PVC) flexible substrate by NPDS, for a TE generator. Here, we focused on the fabrication and characterization of the flexible  $\text{TiO}_2/\text{Sb}_2\text{Te}_3$  TE generator.

## Chapter 2. Experimental procedures

### 2.1 Nanoparticle deposition system

A NPDS was used to deposit TE powders by spraying nano- or microsized particles at room temperature and under low vacuum conditions. Figure 2.1 shows the NPDS system and nozzle used to deposit the TE powder. The nozzle was a slit-type, and the deposition area was  $10 \times 1 \text{ mm}^2$  without moving the nozzle. The deposition parameters are listed in Table 2.1.

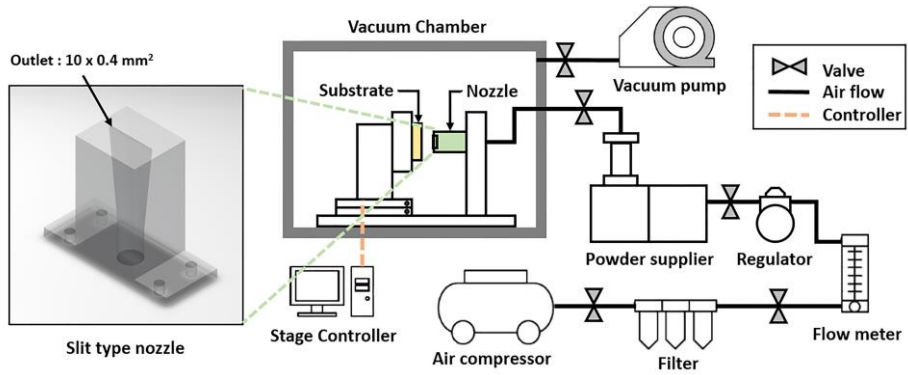


**Figure 2.1.** Schematic diagram of the nanoparticle deposition system (NPDS).

**Table 2.1** Nanoparticle deposition system (NPDS) parameters.

<b>Parameters</b>	<b>Values</b>
Distance between substrate and nozzle	2.5 mm
Compressor pressure	0.28 MPa
Chamber pressure	0.01 MPa
Powder feed rate	0.05 mm/s
Compressed air velocity	300 m/s
Carrier gas	Compressed air

## 2.2 Materials

In the field of TE generator research, TE semiconductor materials with a band structure, high electrical conductivity, and low thermal conductivity have been used to optimize ZT; TE powders commonly used include  $\text{Bi}_2\text{Te}_3$ ,  $\text{Sb}_2\text{Te}_3$ , and  $\text{ZnO}$ . In this research, Sb powder (99.9 % metal basis, -200 mesh, Alfa Aesar) and Te powder (99.8 % metal basis, -200 mesh, Acros Organics) were mixed by agitation with a TE powder. The mixing ratio of Sb and Te was 43:57 by weight.  $\text{TiO}_2$  nanopowder (anatase phase, 15 nm, Nanoamor) was included in the TE powder to improve the adhesion and TE properties. Transparent PVC was used as the flexible substrate and was cut into  $60 \times 20 \text{ mm}^2$  piece, having a thickness of 0.23 mm.

### 2.3 TE generator fabrication process

PVC substrates were cleaned by sonication in ethyl alcohol, and TE film legs were prepared using the dry-spray method (NPDS). Sixteen  $\text{TiO}_2/\text{Sb}_2\text{Te}_3$  TE film legs (length: 10.5 mm; width: 1.2 mm) were deposited at regular intervals by NPDS. Silver (Ag) contacts were used as the electrical interconnects between the legs, which were patterned in series, as shown in Fig. 2.2, using a commercial Ag paste with patterned polyimide masking tape and a scalpel. The series TE legs generate electrical power via the temperature differential between both ends of them.

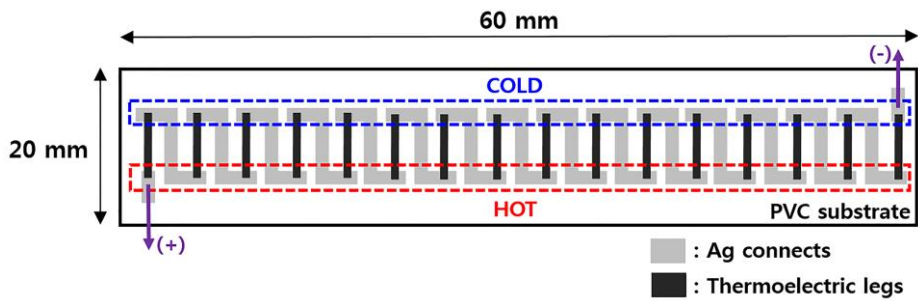


**Figure 2.2.** Schematic diagram of the thermoelectric (TE) generator.

## **2.4 Characterization**

The morphology of the  $\text{TiO}_2/\text{Sb}_2\text{Te}_3$  TE films was examined using field-emission scanning electron microscopy (FE-SEM, SUPRA 55VP), and the phase structure was analyzed by an X-ray diffraction system with monochromatic  $\text{Cu-K}\alpha$  radiation. The Seebeck coefficient of one TE leg was calculated from output voltage and the gradient of the temperature differential which included influence of the thermal conductivity of the TE films. The temperature difference, current, and output voltage were measured by thermocouples and an electrometer (Keithley 6514).

## **Chapter 3. Results and Discussion**

### **3.1 Field-emission scanning electron microscopy**

Figure 3.1 shows SEM images of the surface and cross-section of the  $\text{TiO}_2/\text{Sb}_2\text{Te}_3$  TE films. The images show that particles of varying size and color agglomerated in the film. Following deposition, the white  $\text{TiO}_2$  particles were dispersed between  $\text{Sb}_2\text{Te}_3$  films. The thicknesses of the films were approximately  $60\ \mu\text{m}$ .

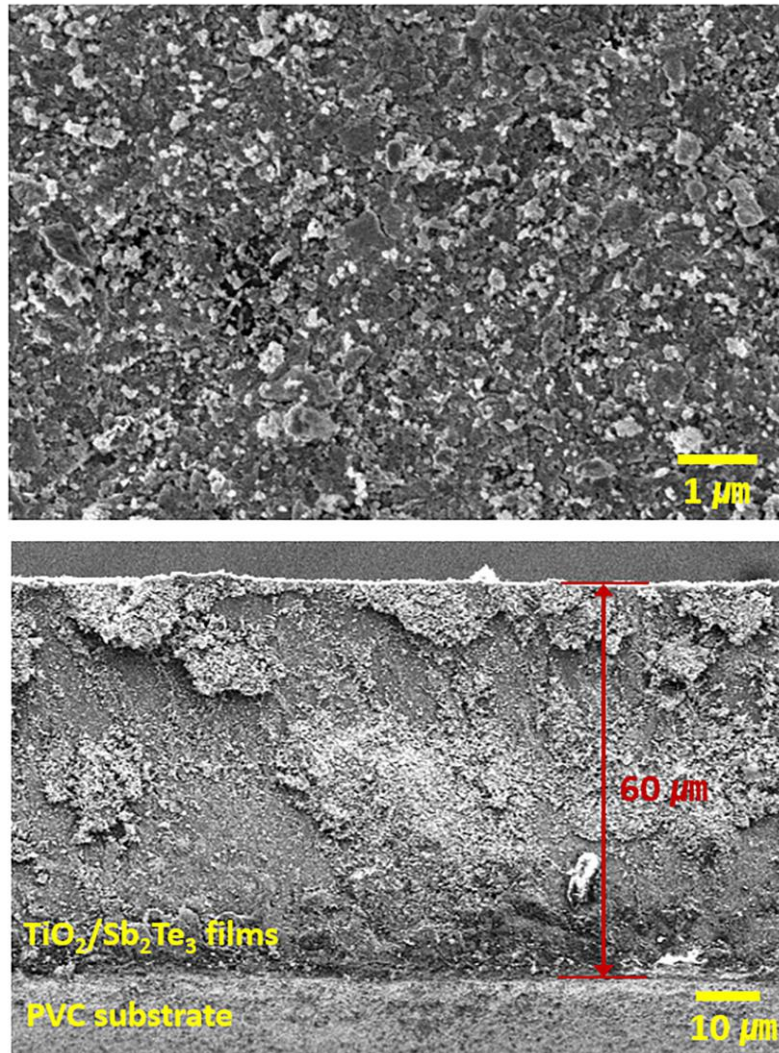


**Figure 3.1.** Scanning electron microscopy (SEM) images of the surface (top) and cross-section (bottom) of the TiO<sub>2</sub>/Sb<sub>2</sub>Te<sub>3</sub> films.

### 3.2 X-ray diffraction

The XRD analysis presented in Fig. 3.2 indicates that the TE powder contained Sb, Te, and  $\text{TiO}_2$  particles. The TE films deposited by NPDS were composed of  $\text{Sb}_2\text{Te}_3$  compound and  $\text{TiO}_2$  particles. Moreover, the XRD peaks of the TE films were broader than those of the TE powder. These results show that the consolidation and fracture of the TE powder during deposition process resulted in a formation of  $\text{Sb}_2\text{Te}_3$  compound and a reduction of the crystallite size in the TE film.

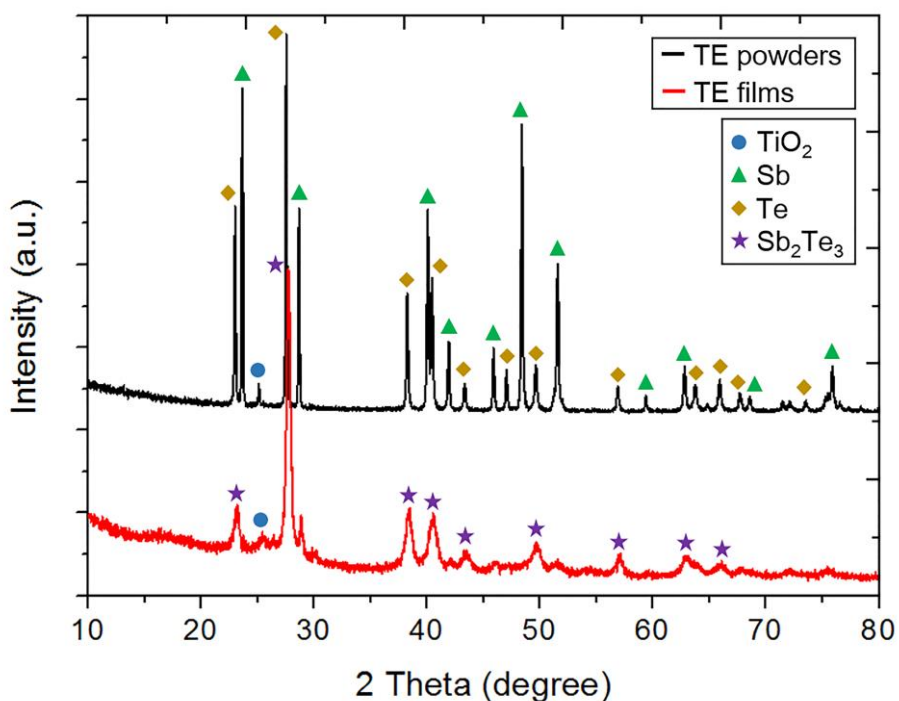


**Figure 3.2.** X-ray diffraction (XRD) patterns of the TE powder and the TE films.

### 3.3 Seebeck coefficient and internal resistance

Figure 3.3 shows the composition ratio of the  $\text{TiO}_2$  dependence of the Seebeck coefficient and internal resistance of one TE leg. The Seebeck coefficient and internal resistance were inversely proportional. At 3 wt%  $\text{TiO}_2$  content, the largest Seebeck coefficient was approximately  $160 \mu\text{V}/\text{K}$ , and the lowest internal resistance of  $0.832 \text{ k}\Omega$  was identified. These results demonstrate that an optimal volume of  $\text{TiO}_2$  enhances the TE properties of the TE film. However, above 3 wt%, the  $\text{TiO}_2$  composition decreased the TE properties owing to its high electrical resistivity. The TE legs of the TE generator were fabricated by TE powder with 3 wt%  $\text{TiO}_2$  contents.

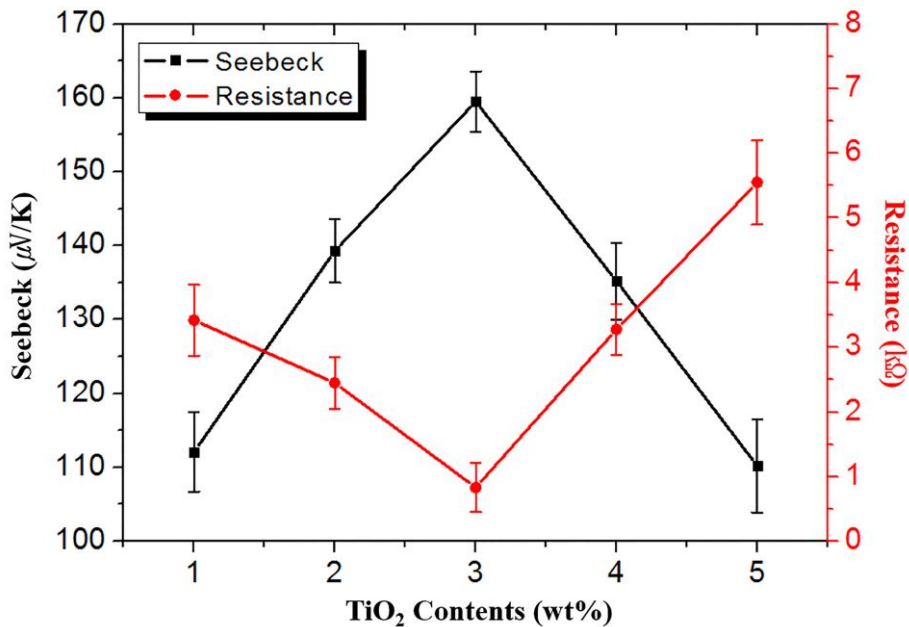


**Figure 3.3.** Seebeck coefficient and internal resistance of one TE leg as a function of the  $\text{TiO}_2$  ratio.

### 3.4 Prototype flexible TE generator

A prototype flexible TE power generator was successfully fabricated, as shown in Fig. 3.4. Sixteen TE legs were connected by Ag connects; the flexible PVC substrate could be bent perpendicular with respect to the TE direction, and the TE legs had sufficient adhesion to the PVC substrate to endure bending.

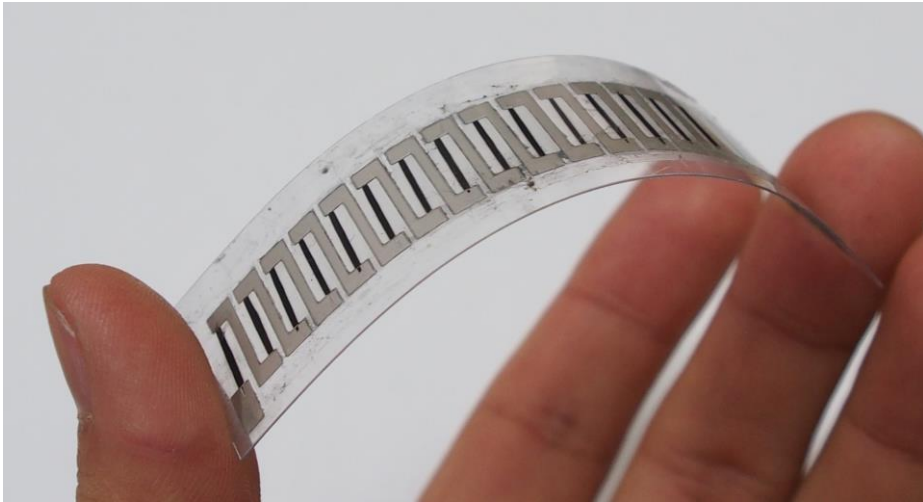


**Figure 3.4.** Image of the flexible TE generator under bending stress.

### 3.5 Voltage and power output

The voltage and power output for the prototype flexible TE power generator were measured as a function of the temperature difference in Fig. 3.5. The inset shows how voltage and current were measured, and how the temperature differential gradient was applied to the end of each leg by a heat sink and hot plate. According to Fig. 3.5, the maximum voltage was 48.91 mV, and the maximum power output was 0.18  $\mu\text{W}$  at  $\Delta T = 20 \text{ K}$ .

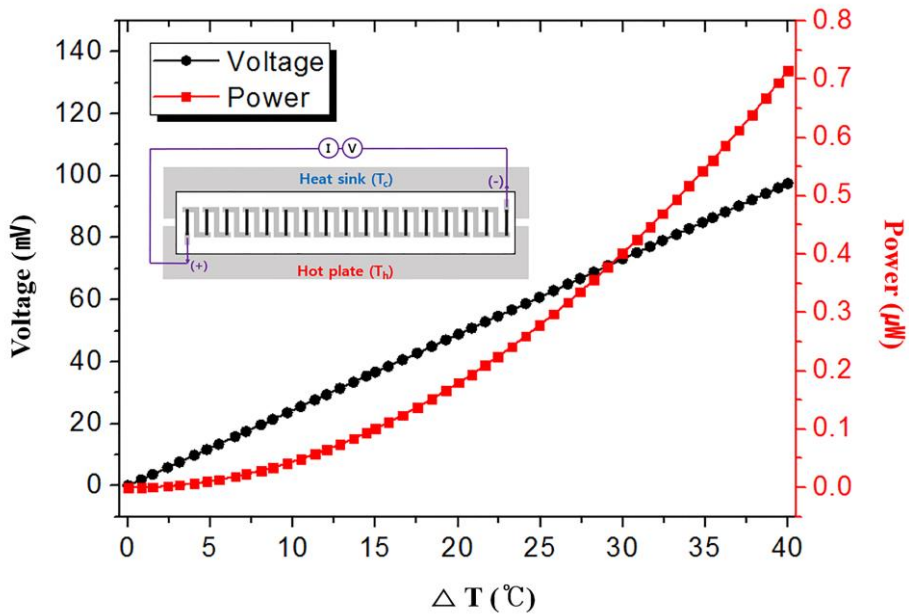


**Figure 3.5.** Voltage and power output for the flexible TE power generator as a function of the temperature differential. The inset shows a schematic of the measurement setup.

### **3.6 Comparison**

Various fabrication processes for flexible TE generators were compared in Table 3.1. Screen printing consume a large amount of energy due to the high annealing temperatures (250°C) and high pressing pressure ( $250 \times 10^6$  Pa) [16], and inkjet printing also need high annealing temperature (400°C) [6]. CVD uses a large amount of energy, due to the growth temperature required (400°C) [7]. Although NPDS operates at room temperature and under low-vacuum conditions (10000 Pa), the TE properties of a generator fabricated by NPDS were comparable to that of a TE generator fabricated by high-energy consumption processes. Therefore, NPDS is a promising new, energy-efficient method for TE generator fabrication.

**Table 3.1.** Comparison of various fabrication processes for flexible TE generators.

Process	NPDS	Screen printing	Inkjet printing	CVD
Materials	<b>TiO<sub>2</sub>/Sb<sub>2</sub>Te<sub>3</sub></b>	Bi <sub>1.8</sub> Te <sub>3.2</sub> , Sb <sub>2</sub> Te <sub>3</sub>	Sb <sub>1.5</sub> Bi <sub>0.5</sub> Te <sub>3</sub> , Bi <sub>2</sub> Te <sub>2.7</sub> Se <sub>0.3</sub>	Bi <sub>2</sub> Te <sub>3</sub> , Bi <sub>0.4</sub> Sb <sub>1.6</sub> Te <sub>3.0</sub>
Substrate	<b>PVC</b>	Polyimide	Polyimide	SiO <sub>2</sub> /GaAs
Temperature (°C)	<b>RT</b>	RT	60	400
Pressure (Pa)	<b>10000 (low vacuum)</b>	250 × 10 <sup>6</sup> (high pressure)	Atmosphere	High vacuum
Annealing (°C)	<b>None</b>	250	400	None
Thickness (μm)	<b>60</b>	78.4	Not specified	4
Seebeck coefficient (μV/K)	<b>160</b>	104	139	230
Maximum power output at ΔT = 20 °C	<b>0.18 μW of power by 16 TE legs</b>	40.3 nW of power by 16 TE junctions	Not specified	0.2 μW of power by 20 pairs of TE legs

NPDS: nanoparticle deposition system; CVD: chemical vapor deposition;  
PVC: polyvinyl chloride.

## Chapter 4. Conclusions

Sixteen  $\text{TiO}_2/\text{Sb}_2\text{Te}_3$  TE legs were patterned on a flexible PVC substrate using NPDS at room temperature and under low-vacuum. To improve the TE properties and adhesion between the film and substrate,  $\text{TiO}_2$  nanopowders were dispersed on the starting TE powders with 3 wt% content. A TE leg, deposited with 3 wt%  $\text{TiO}_2$ , had the highest Seebeck coefficient (about 160  $\mu\text{V}/\text{K}$ ) and the lowest internal resistance of 0.832  $\text{k}\Omega$ . The prototype TE generator produced 0.18  $\mu\text{W}$  at 48.91 mV and 3.68  $\mu\text{A}$  for a temperature difference of 20 K. This value is similar to those of high-energy consumption methods. Therefore, the NPDS provides a novel, energy-efficient means of TE film deposition for eco-friendly fabrication of TE generators. Our future work will focus on decreasing the internal resistance of the module and the contact resistance between the element and electrode for optimizing the power output of the TE generator.

## Reference

- [1] V. Leonov and R. Vullers, *J. Renew. Sust. Energ.* 1, 062701 (2009)
- [2] R. Buchner, K. Froehner, C. Sosna, W. Benecke and W. Lang, *J. Microelectromech. S.* 17, 1114 (2008)
- [3] J.R. Buckle, A. Knox, J. Siviter and A. Montecucco, *J. Electron. Mater.* 42, 2214 (2013)
- [4] S.H. Lee, J.H. Lee, C.W. Park, C.Y. Lee, K.S. Kim, D.H. Tahk and M.K. Kwak, *Int. J. Precis. Eng. Man. Green. Tech.* 1, 119 (2014)
- [5] C. Navone, M. Soulier, M. Plissonnier and A.L. Seiler, *J. Electron. Mater.* 39, 1755 (2010)
- [6] Z. Lu, M. Layani, X. Zhao, L.P. Tan, T. Sun, S. Fan, Q. Yan, S. Magdassi and H.H. Hng, *Small* 10, 3551 (2014)
- [7] S.D. Kwon, B.K. Ju, S.J. Yoon and J.S. Kim, *J. Electron. Mater.* 38, 920 (2009)
- [8] L. Francioso, C.D. Pascali, I. Farella, C. Martucci, P. Cretì, P. Siciliano and A. Perrone, *J. Power. Sources.* 196, 3239 (2011)
- [9] M. Takashiri, T. Shirakawa, K. Miyazaki and H. Tsukamoto, *Sensor. Actuat. A-phys.* 138.2, 329 (2007)
- [10] S.J. Kim, J.H. We and B.J. Cho, *Energ. Environ. Sci* 7, 1959 (2014)

- [11] D.M. Chun, J.O. Choi, Caroline S.Y. Lee, I. Kanno, H. Kotera and S.H. Ahn, *Int. J. Precis. Eng. Man.* 13, 1107 (2012)
- [12] M.H. Kim, K.S. Kim, J.W. Lee, M.S. Kim, J.O. Choi, S.H. Ahn and C.S. Lee, *J. Nanosci. Nanotechno.* 12, 3478 (2012)
- [13] S.I. Park, S.Y. Kim, J.O. Choi, J.H. Song, M.Taya and S.H. Ahn, *Thin Solid Films* 589, 412 (2015)
- [14] H.S. Kim, S.K. Yang, R.C. Pawar, S.H. Ahn and C.S. Lee, *Ceram. Int.* 41, 5937 (2015)
- [15] Y. Zhu, H. Shen and H. Chen, *Rare Metals* 31, 43 (2012)
- [16] Z. Cao, E. Koukharenko, R.N. Torah, J. Tudor and S.P. Beeby, *Journal of Physics: Conference Series*, p 012016. (2014)

## Abstract (Korean)

본 연구에서는 나노 입자 적층 시스템으로 티타늄 다이옥사이드, 안티몬, 그리고 텔루륨 분말을 사용한 유연 열전소자 발전기를 제시하였다. 나노 입자 적층 시스템은 작은 에너지 소비를 갖는 새로운 건식 스프레이 방법으로서, 상온과 저 진공 상태에서 무기물 재료들을 기판에 증착할 수 있다. 티타늄 다이옥사이드 나노 분말들은 열전소자 층과 기판 사이의 접착을 향상시키기 위해 열전소자 분말들에 분산되었다.

증착된 열전소자 층의 모폴로지는 주사전자현미경에 의해 조사하였으며, 상의 구조는 엑스레이 분산을 이용하여 분석하였다. 질량비가 3 w%인 티타늄 다이옥사이드로 증착된 하나의 열전소자 구간은 최대 약  $160 \mu\text{V/K}$ 의 제백 계수를 가졌다. 제작된 열전소자 발전기의 프로토타입은 은 배선으로 연결된 16개의 열전소자 구간들로 이루어졌으며 이 면적은  $20 \times 60 \text{ mm}^2$  였다. 프로토타입은 20 K의 온도 구배 차이에서 48.91 mV의 전압과 최대  $0.18 \mu\text{W}$ 의 전력을 만들 수 있었다. 이 수치들은 기존의 열전소자 발전기 제작 방법으로 제작된 열전소자 발전기의 수치들과 비교할 만하였다. 이 결과들은 유연 열전소자 발전기가 보다 에너지 효율적인 방법으로 제작될 수 있음을 제시하였으나, 내부와 접촉 저항은 개선되어야 한다.

**주요어:** 나노 입자 적층 시스템, 유연 열전소자 발전기, 건식 스프레이 증착, 상온.

**학번:** 2014-21841



저작자표시-비영리-변경금지 2.0 대한민국

이용자는 아래의 조건을 따르는 경우에 한하여 자유롭게

- 이 저작물을 복제, 배포, 전송, 전시, 공연 및 방송할 수 있습니다.

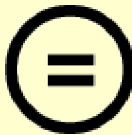
다음과 같은 조건을 따라야 합니다:



저작자표시. 귀하는 원저작자를 표시하여야 합니다.



비영리. 귀하는 이 저작물을 영리 목적으로 이용할 수 없습니다.



변경금지. 귀하는 이 저작물을 개작, 변형 또는 가공할 수 없습니다.

- 귀하는, 이 저작물의 재이용이나 배포의 경우, 이 저작물에 적용된 이용허락조건을 명확하게 나타내어야 합니다.
- 저작권자로부터 별도의 허가를 받으면 이러한 조건들은 적용되지 않습니다.

저작권법에 따른 이용자의 권리는 위의 내용에 의하여 영향을 받지 않습니다.

이것은 [이용허락규약\(Legal Code\)](#)을 이해하기 쉽게 요약한 것입니다.

[Disclaimer](#)

공학석사학위논문

건식 스프레이 증착 시스템을 이용한  
유연 열전소자 발전기 상온 제작

Room-temperature fabrication of  
flexible thermoelectric generator  
using dry-spray deposition system

2016년 2월

서울대학교 대학원

기계항공공학부

송대섭

## Abstract

# Room-temperature fabrication of flexible thermoelectric generator using dry-spray deposition system

Dae-Seob Song

Department of Mechanical and Aerospace Engineering

The Graduate School

Seoul National University

We present a flexible thermoelectric (TE) generator with titanium dioxide ( $\text{TiO}_2$ ), antimony (Sb), and tellurium (Te) powders fabricated by a nanoparticle deposition system (NPDS). NPDS is a novel low-energy consumption dry-spray method that enables the deposition of inorganic materials on substrates at room temperature and under low vacuum.  $\text{TiO}_2$  nanopowders were dispersed on a TE powder for improved adhesion between TE films and the substrate. Film morphologies were investigated using field-emission scanning electron microscopy, and the phase structure was analyzed by X-ray diffraction. A TE leg, deposited with 3 wt%  $\text{TiO}_2$  content, had the largest Seebeck coefficient of approximately  $160 \mu\text{V/K}$ . The prototype TE generator consisted of 16 TE legs linked by silver interconnects over an area of  $20 \times 60 \text{ mm}^2$ . The prototype produced a voltage of 48.91 mV and a

maximum power output of 0.18  $\mu$ W from a temperature gradient of 20 K. The values are comparable to that of conventional methods. These results suggest that flexible TE generators can be fabricated by energy efficient methods, although internal and contact resistances must be decreased.

**Keywords:** nano-particle deposition system, flexible thermoelectric generator, dry-spray deposition, room temperature.

**Student Number:** 2014-21841

# Contents

<b>Chapter 1. Introduction.....</b>	<b>1</b>
1.1 Background.....	1
1.2 Fabrication of flexible TE generators .....	2
1.3 Objectives .....	3
<b>Chapter 2. Experimental procedure.....</b>	<b>4</b>
2.1 Nano particle deposition system.....	4
2.2 Materials .....	6
2.3 TE generator fabrication process .....	7
2.4 Characterization.....	8
<b>Chapter 3. Results and Discussion .....</b>	<b>9</b>
3.1 Field-emission scanning electron microscopy.....	9
3.2 X-ray diffraction .....	11
3.3 Seebeck coefficient and internal resistance .....	12
3.4 Prototype flexible TE generator .....	13
3.5 Voltage and power output .....	14
3.6 Comparison with various fabrication methods .....	15

**Chapter 4. Conclusions.....17**

**Reference.....18**

**Abstract (Korean) .....20**

## **List of Tables**

Table 2.1 Nanoparticle deposition system (NPDS) parameters. ....	5
Table 3.1 Comparison of various fabrication processes for flexible TE generators.....	16

## List of Figures

Figure 2.1 Schematic diagram of the nanoparticle deposition system . . . . .	4
Figure 2.2 Schematic diagram of the thermoelectric (TE) generator . . . . .	7
Figure 3.1 Scanning electron microscopy (SEM) images of the surface (top) and cross-section (bottom) of the $\text{TiO}_2/\text{Sb}_2\text{Te}_3$ films. . . . .	10
Figure 3.2 X-ray diffraction (XRD) patterns of the TE powder and the TE films. . . . .	11
Figure 3.3 Seebeck coefficient and internal resistance of one TE leg as a function of the $\text{TiO}_2$ ratio. . . . .	12
Figure 3.4 Image of the flexible TE generator under bending stress . . . . .	13
Figure 3.5 Voltage and power output for the flexible TE power generator as a function of the temperature differential. The inset shows a schematic of the measurement setup. . . . .	14

# **Chapter 1. Introduction**

## **1.1 Background**

Thermoelectric (TE) power generators convert a thermal differential into electrical power and can be used to improve energy consumption efficiency. Moreover, flexible TE power generators can be used in self-powered portable electronic systems, such as wearable electronics, biometric sensors, and autonomous robots [1–4].

## 1.2 Fabrication of flexible TE generator

Recently, various TE materials and manufacturing methods have been developed for the fabrication of flexible TE generators. TE materials based on tellurium (Te) and antimony (Sb) have typically been used for this purpose, due to their high figure of merit values,  $ZT$ , where  $ZT = \alpha^2 \cdot T / \rho \cdot \lambda$ ,  $\lambda$  is the thermal conductivity,  $\rho$  is the electrical resistivity,  $\alpha$  is the Seebeck coefficient, and  $T$  is the temperature; the printing methods utilized (e.g., screen printing [5], inkjet printing [6], metal organic chemical vapor deposition (MOCVD) [7], co-sputtering [8], and flash evaporation [9]) significantly improved the energy conversion efficiency of the TE generators. A glass fabric-based flexible TE generator, which was recently optimized and developed for wearable mobile electronic systems, showed remarkable output power, but also high energy consumption and cost [10]. Pastes which contain TE and binder materials for screen printing and inkjet printing must be annealed. Also, MOCVD consumes a large amount of energy, due to the high growth temperatures required. Co-sputtering and flash evaporation methods require a post-annealing process to improve the TE generator's performance. These high-energy processes negate the benefits of TE generators; thus, more efficient fabrication processes are required for widespread adoption.

### 1.3 Objectives

The nanoparticle deposition system (NPDS), which can deposit metal and ceramic particles using a dry-spray process at room temperature and under low-vacuum conditions, was developed by Ahn et al. in 2006. NPDS is similar to the aerosol deposition method (ADM); however, NPDS is a relatively low-energy consumption process, compared with alternative dry-spray processes [11]. NPDS requires a low-pressure gas carrier and a low vacuum, which reduces energy consumption and the complexity of the facilities needed. NPDS has been used to deposit  $\text{TiO}_2$  and  $\text{WO}_3$  particles on a substrate for energy applications, such as dye-sensitized solar cells (DSSC) and electrochromic displays [12,13], which suggests the use of a NPDS for efficient fabrication of flexible TE generators.

According to a recent study, microparticles with a  $\text{TiO}_2$  nanopowder deposited by NPDS adhered well to the substrate and exhibited a greater film density than other pure microsized particles [14]. In addition,  $\text{TiO}_2$  nanopowders dispersed in TE materials may result in remarkable phonon scattering, reducing thermal conductivity [15].

In the present work, we fabricated 16  $\text{Sb}_2\text{Te}_3$  TE film (p-type) legs, with a  $\text{TiO}_2$  nanopowder, dispersed on a polyvinyl chloride (PVC) flexible substrate by NPDS, for a TE generator. Here, we focused on the fabrication and characterization of the flexible  $\text{TiO}_2/\text{Sb}_2\text{Te}_3$  TE generator.

## Chapter 2. Experimental procedures

### 2.1 Nanoparticle deposition system

A NPDS was used to deposit TE powders by spraying nano- or microsized particles at room temperature and under low vacuum conditions. Figure 2.1 shows the NPDS system and nozzle used to deposit the TE powder. The nozzle was a slit-type, and the deposition area was  $10 \times 1 \text{ mm}^2$  without moving the nozzle. The deposition parameters are listed in Table 2.1.

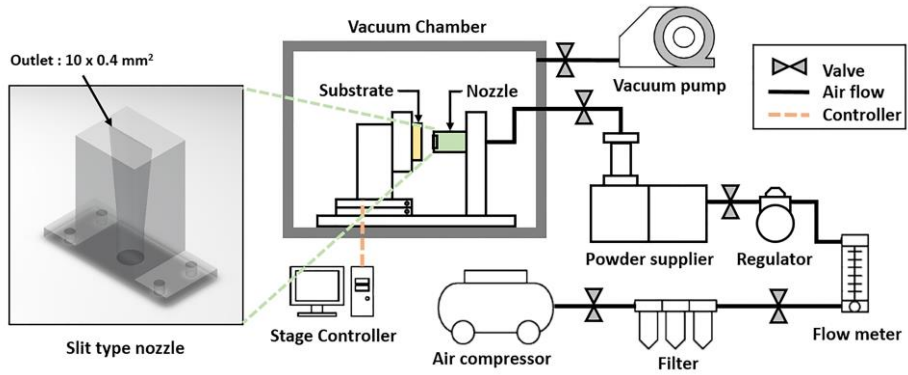


**Figure 2.1.** Schematic diagram of the nanoparticle deposition system (NPDS).

**Table 2.1** Nanoparticle deposition system (NPDS) parameters.

<b>Parameters</b>	<b>Values</b>
Distance between substrate and nozzle	2.5 mm
Compressor pressure	0.28 MPa
Chamber pressure	0.01 MPa
Powder feed rate	0.05 mm/s
Compressed air velocity	300 m/s
Carrier gas	Compressed air

## 2.2 Materials

In the field of TE generator research, TE semiconductor materials with a band structure, high electrical conductivity, and low thermal conductivity have been used to optimize ZT; TE powders commonly used include  $\text{Bi}_2\text{Te}_3$ ,  $\text{Sb}_2\text{Te}_3$ , and  $\text{ZnO}$ . In this research, Sb powder (99.9 % metal basis, -200 mesh, Alfa Aesar) and Te powder (99.8 % metal basis, -200 mesh, Acros Organics) were mixed by agitation with a TE powder. The mixing ratio of Sb and Te was 43:57 by weight.  $\text{TiO}_2$  nanopowder (anatase phase, 15 nm, Nanoamor) was included in the TE powder to improve the adhesion and TE properties. Transparent PVC was used as the flexible substrate and was cut into  $60 \times 20 \text{ mm}^2$  piece, having a thickness of 0.23 mm.

### 2.3 TE generator fabrication process

PVC substrates were cleaned by sonication in ethyl alcohol, and TE film legs were prepared using the dry-spray method (NPDS). Sixteen  $\text{TiO}_2/\text{Sb}_2\text{Te}_3$  TE film legs (length: 10.5 mm; width: 1.2 mm) were deposited at regular intervals by NPDS. Silver (Ag) contacts were used as the electrical interconnects between the legs, which were patterned in series, as shown in Fig. 2.2, using a commercial Ag paste with patterned polyimide masking tape and a scalpel. The series TE legs generate electrical power via the temperature differential between both ends of them.

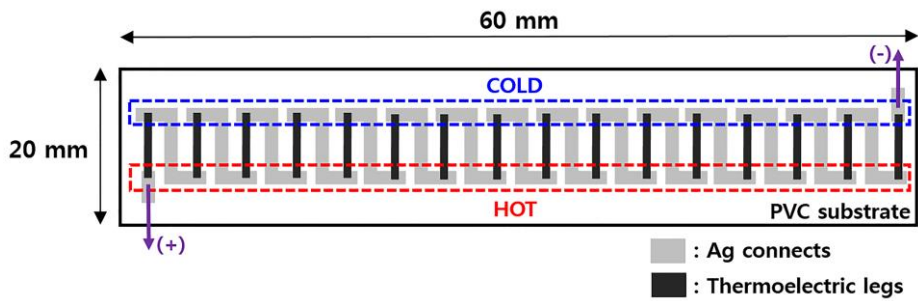


**Figure 2.2.** Schematic diagram of the thermoelectric (TE) generator.

## **2.4 Characterization**

The morphology of the  $\text{TiO}_2/\text{Sb}_2\text{Te}_3$  TE films was examined using field-emission scanning electron microscopy (FE-SEM, SUPRA 55VP), and the phase structure was analyzed by an X-ray diffraction system with monochromatic  $\text{Cu-K}\alpha$  radiation. The Seebeck coefficient of one TE leg was calculated from output voltage and the gradient of the temperature differential which included influence of the thermal conductivity of the TE films. The temperature difference, current, and output voltage were measured by thermocouples and an electrometer (Keithley 6514).

## **Chapter 3. Results and Discussion**

### **3.1 Field-emission scanning electron microscopy**

Figure 3.1 shows SEM images of the surface and cross-section of the  $\text{TiO}_2/\text{Sb}_2\text{Te}_3$  TE films. The images show that particles of varying size and color agglomerated in the film. Following deposition, the white  $\text{TiO}_2$  particles were dispersed between  $\text{Sb}_2\text{Te}_3$  films. The thicknesses of the films were approximately  $60\ \mu\text{m}$ .

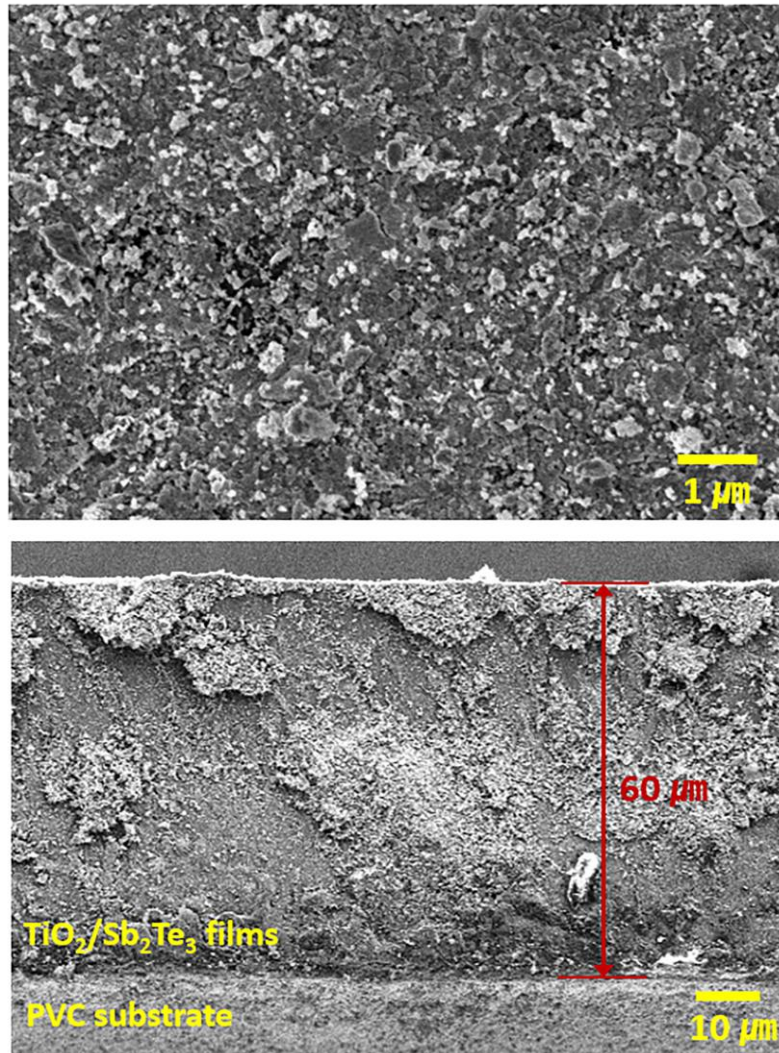


**Figure 3.1.** Scanning electron microscopy (SEM) images of the surface (top) and cross-section (bottom) of the TiO<sub>2</sub>/Sb<sub>2</sub>Te<sub>3</sub> films.

### 3.2 X-ray diffraction

The XRD analysis presented in Fig. 3.2 indicates that the TE powder contained Sb, Te, and  $\text{TiO}_2$  particles. The TE films deposited by NPDS were composed of  $\text{Sb}_2\text{Te}_3$  compound and  $\text{TiO}_2$  particles. Moreover, the XRD peaks of the TE films were broader than those of the TE powder. These results show that the consolidation and fracture of the TE powder during deposition process resulted in a formation of  $\text{Sb}_2\text{Te}_3$  compound and a reduction of the crystallite size in the TE film.

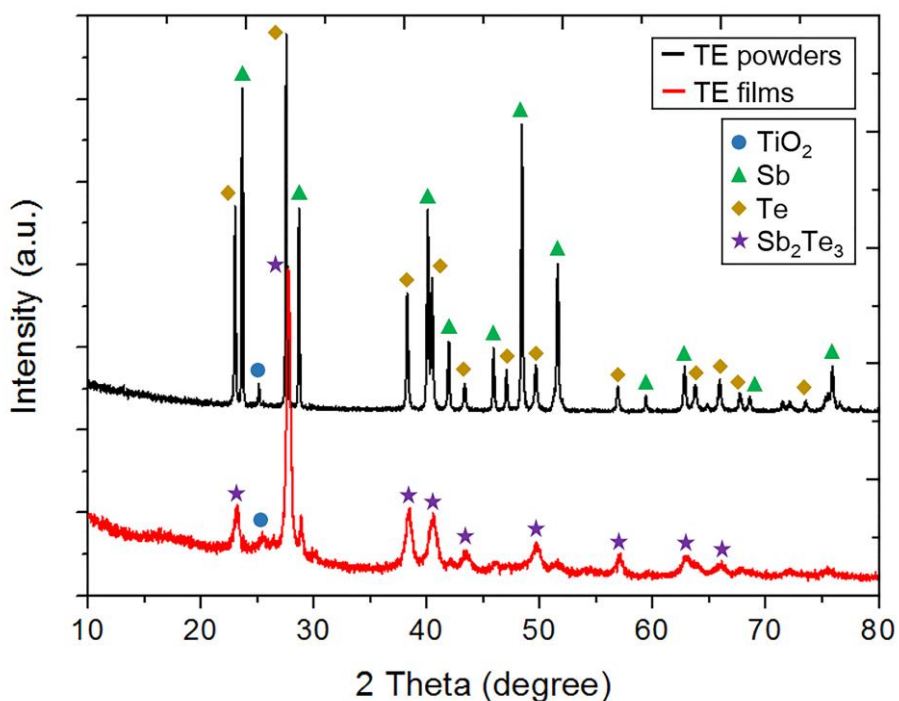


**Figure 3.2.** X-ray diffraction (XRD) patterns of the TE powder and the TE films.

### 3.3 Seebeck coefficient and internal resistance

Figure 3.3 shows the composition ratio of the  $\text{TiO}_2$  dependence of the Seebeck coefficient and internal resistance of one TE leg. The Seebeck coefficient and internal resistance were inversely proportional. At 3 wt%  $\text{TiO}_2$  content, the largest Seebeck coefficient was approximately  $160 \mu\text{V}/\text{K}$ , and the lowest internal resistance of  $0.832 \text{ k}\Omega$  was identified. These results demonstrate that an optimal volume of  $\text{TiO}_2$  enhances the TE properties of the TE film. However, above 3 wt%, the  $\text{TiO}_2$  composition decreased the TE properties owing to its high electrical resistivity. The TE legs of the TE generator were fabricated by TE powder with 3 wt%  $\text{TiO}_2$  contents.

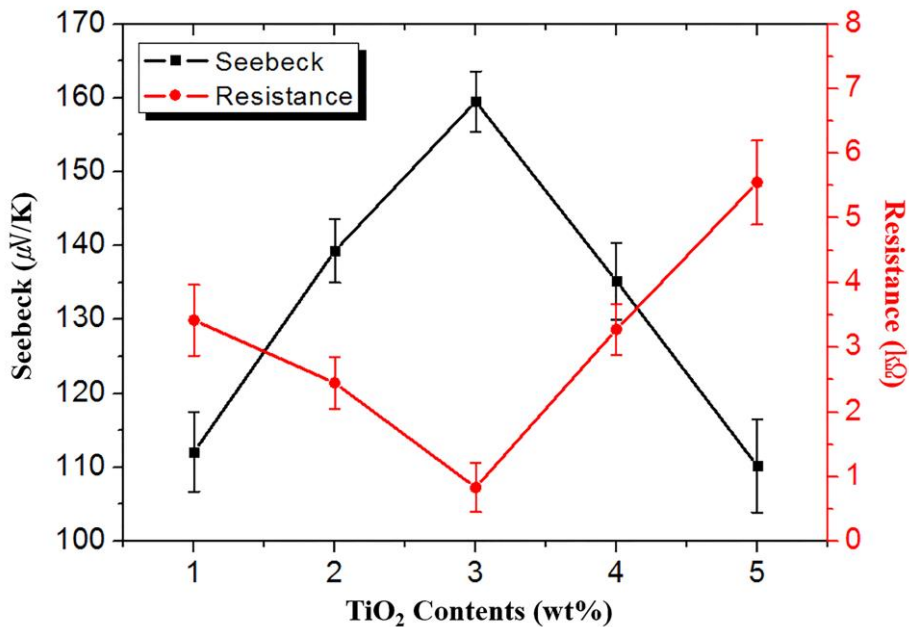


**Figure 3.3.** Seebeck coefficient and internal resistance of one TE leg as a function of the  $\text{TiO}_2$  ratio.

### 3.4 Prototype flexible TE generator

A prototype flexible TE power generator was successfully fabricated, as shown in Fig. 3.4. Sixteen TE legs were connected by Ag connects; the flexible PVC substrate could be bent perpendicular with respect to the TE direction, and the TE legs had sufficient adhesion to the PVC substrate to endure bending.



**Figure 3.4.** Image of the flexible TE generator under bending stress.

### 3.5 Voltage and power output

The voltage and power output for the prototype flexible TE power generator were measured as a function of the temperature difference in Fig. 3.5. The inset shows how voltage and current were measured, and how the temperature differential gradient was applied to the end of each leg by a heat sink and hot plate. According to Fig. 3.5, the maximum voltage was 48.91 mV, and the maximum power output was 0.18  $\mu\text{W}$  at  $\Delta T = 20 \text{ K}$ .

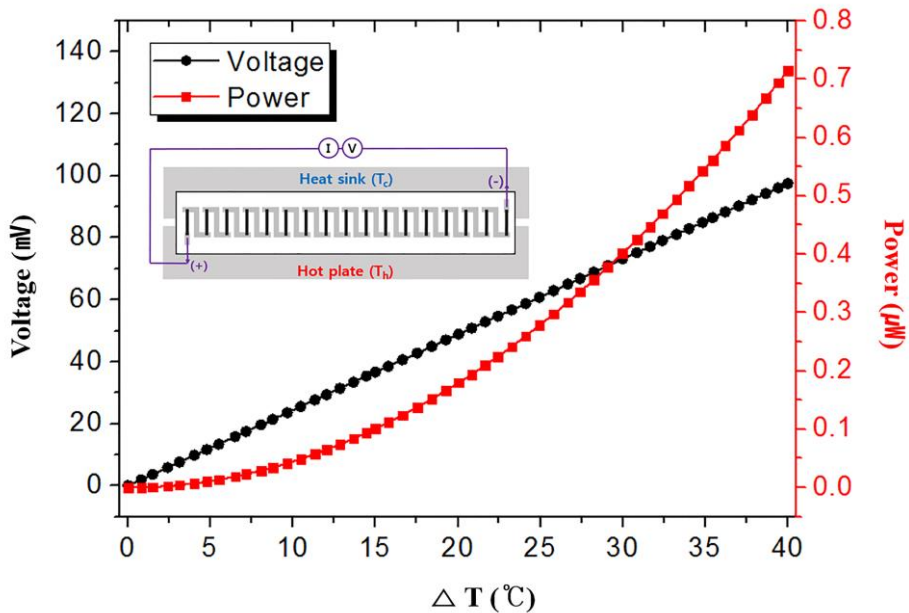


**Figure 3.5.** Voltage and power output for the flexible TE power generator as a function of the temperature differential. The inset shows a schematic of the measurement setup.

### **3.6 Comparison**

Various fabrication processes for flexible TE generators were compared in Table 3.1. Screen printing consume a large amount of energy due to the high annealing temperatures (250°C) and high pressing pressure ( $250 \times 10^6$  Pa) [16], and inkjet printing also need high annealing temperature (400°C) [6]. CVD uses a large amount of energy, due to the growth temperature required (400°C) [7]. Although NPDS operates at room temperature and under low-vacuum conditions (10000 Pa), the TE properties of a generator fabricated by NPDS were comparable to that of a TE generator fabricated by high-energy consumption processes. Therefore, NPDS is a promising new, energy-efficient method for TE generator fabrication.

**Table 3.1.** Comparison of various fabrication processes for flexible TE generators.

Process	NPDS	Screen printing	Inkjet printing	CVD
Materials	<b>TiO<sub>2</sub>/Sb<sub>2</sub>Te<sub>3</sub></b>	Bi <sub>1.8</sub> Te <sub>3.2</sub> , Sb <sub>2</sub> Te <sub>3</sub>	Sb <sub>1.5</sub> Bi <sub>0.5</sub> Te <sub>3</sub> , Bi <sub>2</sub> Te <sub>2.7</sub> Se <sub>0.3</sub>	Bi <sub>2</sub> Te <sub>3</sub> , Bi <sub>0.4</sub> Sb <sub>1.6</sub> Te <sub>3.0</sub>
Substrate	<b>PVC</b>	Polyimide	Polyimide	SiO <sub>2</sub> /GaAs
Temperature (°C)	<b>RT</b>	RT	60	400
Pressure (Pa)	<b>10000 (low vacuum)</b>	250 × 10 <sup>6</sup> (high pressure)	Atmosphere	High vacuum
Annealing (°C)	<b>None</b>	250	400	None
Thickness (μm)	<b>60</b>	78.4	Not specified	4
Seebeck coefficient (μV/K)	<b>160</b>	104	139	230
Maximum power output at ΔT = 20 °C	<b>0.18 μW of power by 16 TE legs</b>	40.3 nW of power by 16 TE junctions	Not specified	0.2 μW of power by 20 pairs of TE legs

NPDS: nanoparticle deposition system; CVD: chemical vapor deposition;  
PVC: polyvinyl chloride.

## Chapter 4. Conclusions

Sixteen  $\text{TiO}_2/\text{Sb}_2\text{Te}_3$  TE legs were patterned on a flexible PVC substrate using NPDS at room temperature and under low-vacuum. To improve the TE properties and adhesion between the film and substrate,  $\text{TiO}_2$  nanopowders were dispersed on the starting TE powders with 3 wt% content. A TE leg, deposited with 3 wt%  $\text{TiO}_2$ , had the highest Seebeck coefficient (about 160  $\mu\text{V}/\text{K}$ ) and the lowest internal resistance of 0.832  $\text{k}\Omega$ . The prototype TE generator produced 0.18  $\mu\text{W}$  at 48.91 mV and 3.68  $\mu\text{A}$  for a temperature difference of 20 K. This value is similar to those of high-energy consumption methods. Therefore, the NPDS provides a novel, energy-efficient means of TE film deposition for eco-friendly fabrication of TE generators. Our future work will focus on decreasing the internal resistance of the module and the contact resistance between the element and electrode for optimizing the power output of the TE generator.

## Reference

- [1] V. Leonov and R. Vullers, *J. Renew. Sust. Energ.* 1, 062701 (2009)
- [2] R. Buchner, K. Froehner, C. Sosna, W. Benecke and W. Lang, *J. Microelectromech. S.* 17, 1114 (2008)
- [3] J.R. Buckle, A. Knox, J. Siviter and A. Montecucco, *J. Electron. Mater.* 42, 2214 (2013)
- [4] S.H. Lee, J.H. Lee, C.W. Park, C.Y. Lee, K.S. Kim, D.H. Tahk and M.K. Kwak, *Int. J. Precis. Eng. Man. Green. Tech.* 1, 119 (2014)
- [5] C. Navone, M. Soulier, M. Plissonnier and A.L. Seiler, *J. Electron. Mater.* 39, 1755 (2010)
- [6] Z. Lu, M. Layani, X. Zhao, L.P. Tan, T. Sun, S. Fan, Q. Yan, S. Magdassi and H.H. Hng, *Small* 10, 3551 (2014)
- [7] S.D. Kwon, B.K. Ju, S.J. Yoon and J.S. Kim, *J. Electron. Mater.* 38, 920 (2009)
- [8] L. Francioso, C.D. Pascali, I. Farella, C. Martucci, P. Cretì, P. Siciliano and A. Perrone, *J. Power. Sources.* 196, 3239 (2011)
- [9] M. Takashiri, T. Shirakawa, K. Miyazaki and H. Tsukamoto, *Sensor. Actuat. A-phys.* 138.2, 329 (2007)
- [10] S.J. Kim, J.H. We and B.J. Cho, *Energ. Environ. Sci* 7, 1959 (2014)

- [11] D.M. Chun, J.O. Choi, Caroline S.Y. Lee, I. Kanno, H. Kotera and S.H. Ahn, *Int. J. Precis. Eng. Man.* 13, 1107 (2012)
- [12] M.H. Kim, K.S. Kim, J.W. Lee, M.S. Kim, J.O. Choi, S.H. Ahn and C.S. Lee, *J. Nanosci. Nanotechno.* 12, 3478 (2012)
- [13] S.I. Park, S.Y. Kim, J.O. Choi, J.H. Song, M.Taya and S.H. Ahn, *Thin Solid Films* 589, 412 (2015)
- [14] H.S. Kim, S.K. Yang, R.C. Pawar, S.H. Ahn and C.S. Lee, *Ceram. Int.* 41, 5937 (2015)
- [15] Y. Zhu, H. Shen and H. Chen, *Rare Metals* 31, 43 (2012)
- [16] Z. Cao, E. Koukharenko, R.N. Torah, J. Tudor and S.P. Beeby, *Journal of Physics: Conference Series*, p 012016. (2014)

## Abstract (Korean)

본 연구에서는 나노 입자 적층 시스템으로 티타늄 다이옥사이드, 안티몬, 그리고 텔루륨 분말을 사용한 유연 열전소자 발전기를 제시하였다. 나노 입자 적층 시스템은 작은 에너지 소비를 갖는 새로운 건식 스프레이 방법으로서, 상온과 저 진공 상태에서 무기물 재료들을 기판에 증착할 수 있다. 티타늄 다이옥사이드 나노 분말들은 열전소자 층과 기판 사이의 접착을 향상시키기 위해 열전소자 분말들에 분산되었다.

증착된 열전소자 층의 모폴로지는 주사전자현미경에 의해 조사하였으며, 상의 구조는 엑스레이 분산을 이용하여 분석하였다. 질량비가 3 w%인 티타늄 다이옥사이드로 증착된 하나의 열전소자 구간은 최대 약  $160 \mu\text{V/K}$ 의 제백 계수를 가졌다. 제작된 열전소자 발전기의 프로토타입은 은 배선으로 연결된 16개의 열전소자 구간들로 이루어졌으며 이 면적은  $20 \times 60 \text{ mm}^2$  였다. 프로토타입은 20 K의 온도 구배 차이에서 48.91 mV의 전압과 최대  $0.18 \mu\text{W}$ 의 전력을 만들 수 있었다. 이 수치들은 기존의 열전소자 발전기 제작 방법으로 제작된 열전소자 발전기의 수치들과 비교할 만하였다. 이 결과들은 유연 열전소자 발전기가 보다 에너지 효율적인 방법으로 제작될 수 있음을 제시하였으나, 내부와 접촉 저항은 개선되어야 한다.

**주요어:** 나노 입자 적층 시스템, 유연 열전소자 발전기, 건식 스프레이 증착, 상온.

**학번:** 2014-21841